



The impact of earthquakes on orogen-scale exhumation

Oliver R Francis^{1,2,*}, Tristram C Hales^{1,2}, Daniel E J Hopley¹, Xuanmei Fan³, Alexander J Horton¹,
Gianvito Scaringi⁴, Runqiu Huang³

5

¹School of Earth and Ocean Sciences, Cardiff university, Main Building, Park Place, Cardiff CF10 3AT

²Sustainable Places Research Institute, Cardiff University 33 Park Place, Cardiff CF10 3BA

³The State Key Laboratory of Geohazard Prevention and Geoenvironment Protection, Chengdu University of Technology, Chengdu 610059, Sichuan, China

10 ⁴Institute of Hydrogeology, Engineering Geology and Applied Geophysics, Faculty of Science, Charles University, Albertov 6, 128 46 Prague 2, Prague, Czech Republic

Correspondence to: O R Francis (Franciso1@cardiff.ac.uk)

Abstract. Individual, large thrusting earthquakes can cause hundreds to thousands of years of exhumation in a geologically instantaneous moment through landslide generation. The bedrock landslides generated are important weathering agents through the conversion of bedrock into mobile sediment. Despite this, records of surface uplift and exhumation at the orogen scale contain little to no evidence of individual large earthquakes. We examine how earthquakes influence exhumation rates by exploring how stochastic earthquakes and landslides affect surface uplift and exhumation in a zero-dimensional numerical model, supported by observations from the 2008 M_w 7.9 Wenchuan earthquake. Our model uses empirically constrained seismic, weathering, and landsliding scaling laws to show that large earthquakes generate the most surface uplift, despite causing exhumation of the bedrock surface. Where earthquakes, rather than aseismic processes predominantly drive rock uplift, rapid surface uplift can occur when regolith is preserved in the orogen, which limits the amount of bedrock weathering. By simulating the concentration of cosmogenic radionuclides within the model domain, we can examine the timescales over which earthquake-driven changes in exhumation can be measured. After an initial lowering in well-mixed landslide material, the concentration of ^{10}Be returns to the long-term average within 10^3 years. We further demonstrate that the variability in exhumation caused by earthquakes occurs at timescales shorter than the averaging time of most thermochronometers. When combined with evidence of signal shredding response within recent earthquakes, it seems unlikely for single earthquakes to affect long-term measurements of exhumation rates. Nevertheless, short term stochastic

15
20
25



feedbacks between weathering and exhumation produce measurable increases in cosmogenically measured exhumation rates which can be linked to earthquakes.

30 1. Introduction

Large, high-relief mountain belts are found along highly active thrust faults, which produce some of the largest and most dangerous earthquakes on the planet (Avouac, 2007; Roback et al., 2018; Stolle et al., 2017). Thrust earthquakes generate uplift by thickening the crust (Avouac, 2007; England and Molnar, 1990), while also producing widespread landsliding (Keefer, 1994; Malamud et al., 2004). Existing mass balances on single (Parker et al., 2011) or sequences (Li et al., 2014, 35 2019; Marc et al., 2016b) of earthquakes demonstrate that landslide volumes of large thrust earthquakes are comparable to, and may exceed, rock uplift. However, earthquakes are not the only rock uplift process in mountain belts; aseismic mechanisms such as viscous and elastic crustal deformation (Meade, 2010; Simpson, 2015), lithospheric delamination (Hales et al., 2005; Molnar et al., 1993), and others (Molnar, 2012; Molnar et al., 2015) can also contribute. The total time-averaged mass balance, and hence surface uplift, is also affected by weathering and erosion between earthquakes (Hovius et al., 2011; 40 Marc et al., 2019; Yanites et al., 2010). Therefore, the contribution of earthquakes to the generation of long-term surface uplift of mountains remains poorly constrained (England and Molnar, 1990; Li et al., 2019). Surface uplift of a mountain range through time is set by the balance of additive uplift processes and removal of material by surface, typically fluvial, processes. Earthquakes along thrust belts produce rock uplift and equally importantly generate exhumation via landsliding. Landsliding events can scour deeply into bedrock, causing many hundreds or thousands of years of exhumation in a geologically instantaneous moment (Li et al., 2014; Marc et al., 2019; Parker et al., 2011; Stolle et al., 2017) – provided we 45 consider the surface towards which exhumation occurs to be the bedrock surface, rather than the topographic surface.

Despite the importance of earthquake-triggered landslides in the total weathering budget of mountain belts, there is little evidence of large earthquakes in the sedimentary or exhumation records. Increased rates of sedimentation and changes in sedimentary characteristics, linked to the abundance of loose sediment, have been identified in lakes and reservoirs immediately proximal to large faults (Howarth et al., 2012; Zhang et al., 2019). However, these pulses in sedimentation may 50 be difficult to separate from extreme hydrological events (Zhang et al., 2019). Steep slopes within mountain belts, as well as typical observations of plentiful exposed bedrock on those slopes, have been used to support the idea that earthquake-generated sediment is rapidly removed from orogenic belts (Dingle et al., 2018; Li et al., 2014; Niemi et al., 2005; Parker et al., 2011). However, observations collected after earthquakes suggests that regolith remains in low-order catchments (Pearce 55 et al., 1986) or in single large landslides (Korup and Clague, 2009; Stolle et al., 2017) for at least hundreds of years. The slow stochastic remobilisation of this sediment from mountain belts by belts by non-linear debris flow and flooding processes and the likely signal shredding maybe one reason why single earthquakes are not recorded (Jerolmack and Paola, 2010). The long return times of the largest earthquakes and the short recording time of cosmogenic radionuclides has been linked to the difference of recorded erosion rates between cosmogenic radionuclides and low temperature



60 **Thermochronometry (Ouimet, 2010).** After the 2008 Wenchuan earthquake detrital cosmogenic nuclide concentrations were lowered, correlating with coseismic landslide density (West et al., 2014). **Landslides impacting local apparent erosion rates suggests a methodology for identifying earthquakes and coseismic material within landscapes.**

In this paper we examine how bedrock **weathering** by stochastic earthquake-triggered landslides (EQTLs) affects exhumation and surface uplift at orogenic scales. We explicitly separate the role of EQTLs generating regolith by *weathering* 65 bedrock from their role as (inefficient) *eroders* of bedrock and regolith – i.e., we separate their role in **producing loose material** from their role in transporting that material. EQTLs occur mostly on hillslopes, typically having transport lengths **consistent with hillslope lengths, with only the largest impinging on the fluvial system** (Li et al., 2016). EQTLs have been argued to be **efficient agents of bedrock weathering** due to their propensity to have depths greater than any existing regolith cover (Larsen et al., 2010) (Figure 1). The amount of weathering performed by a particular earthquake depends on the **size-** 70 **frequency distribution** of these landslides, reflecting a complex interaction between topography, shaking, and material properties of the bedrock (Keefer, 1994; Malamud et al., 2004; Marc et al., 2016a). We investigate the interaction between coseismic rock uplift, regolith generation, and **surface** uplift using a volume balance model. By tracking the bedrock surface through time, we can model both exhumation and denudation and how they are affected by varying earthquake distributions. We also model the concentration of cosmogenic radionuclides in sampled regolith **in order** to compare the modelled result 75 with a global database of cosmogenic nuclide denudation records **in order to** identify the long- and short-term impacts of earthquakes on mountainous landscapes.

1.1 Definitions of terms

This manuscript is precise in its use of terminology around change in elevation of the various surfaces we discuss. These follow standard modern definitions (England and Molnar, 1990; Heimsath et al., 1997), but as we are explicitly measuring 80 the generation of regolith and the movement of two surfaces (the topographic surface and the bedrock surface), the potential for ambiguity requires us to clearly define these terms:

Erosion is the transport away of material, and thus, a change in the topography. In our context, it describes the full evacuation of regolith material from the model domain.

85 **Weathering** is the in-situ conversion of rock into regolith. In our model, rock must be converted to regolith before it can be transported.

Regolith is the mobile transportable layer of sediment at the surface. Regolith can be created by two distinct weathering mechanisms; **landslides cutting into bedrock to create transportable debris**, and soil production by physiochemical processes.

90 **Uplift** is the increase in elevation of a material or surface in an absolute frame of reference. **We distinguish rock uplift, topographic surface uplift, and bedrock surface uplift.**



Exhumation is the approach of the rock mass towards the topographic surface and/or the bedrock surface, in the frame of reference of that surface. Our model tracks both surfaces, so therefore it is possible to have a rock uplift event that causes exhumation at the bedrock surface without exhumation at the topographic surface, by thickening the regolith.

95 **Denudation** is used almost as a synonym for exhumation, but where the frame of reference is the rock mass or the bedrock surface, and the topographic surface moves towards it.

2. Methods

2.1 0-Dimensional Volume Balance Model

100 Here we present a generalised 0-dimensional mountain volume balance model which we use to test the impact of regolith storage on bedrock surface uplift and exhumation. In the absence of sufficient empirical evidence on the long-term spatial distribution of rock uplift, exhumation, and regolith volumes in mountain ranges, we simulate these parameters by treating the evolution of a landscape as a series of dimensionless seismic volume balances. We define the change in topographic surface (S_T) with time as

$$\frac{dS_T}{dt} = U - E \quad (1),$$

105 where U (units of L/T) is the **thickness of rock** entering the orogen and resulting in uplift (calculated as the volume entering the orogen across the area of the model per unit time), while E is the rate of regolith removed from the **topographic surface** and thus is the long-term erosion rate of the orogen. Rock can enter the orogen in two ways, either via shortening and thickening of the crust during coseismic thrusting earthquakes (U_{co}) or through one of a number of aseismic uplift mechanisms (U_{as}), such as lower crustal flow (Royden et al., 1997) or lithospheric delamination (Hales et al., 2005). Surface
110 deformation (Bonilla et al., 1984; Wells and CopperSmith, Kevin, 1994), and hence the volume of rock uplifted, scales as a function of earthquake magnitude (Li et al., 2014; Marc et al., 2016b), which is adjusted for isostatic compensation based on local flexural isostatic calculations (Densmore et al., 2012; Molnar, 2012; Turcotte and Schubert, 2002). We do not consider interseismic strain as a uplifting mechanism in this model due its limited contribution to permanent surface deformation (Avouac, 2007). There is ongoing debate as to the specific mechanisms of aseismic uplift that occur in mountains (Hubbard
115 and Shaw, 2009; Royden et al., 1997), and aseismic uplift can occur both through changes in crustal thickness or changes in the density distribution in the lithosphere, we simplify the aseismic component of uplift and generalise it as the proportion of uplift that cannot be accounted for by U_{co} . Hence, topographic surface uplift can be represented as

$$\frac{dS_T}{dt} = U_{co} + U_{as} - E \quad (2),$$



Where the ratio between U_{as} and U_{co} is defined by α which represents the proportion of the total uplift rate that is caused by aseismic uplift, such that $(1 - \alpha) U = U_{co}$ and $\alpha U = U_{as}$. On long timescales (across many earthquakes), we can describe the sediment flux leaving an orogen as a function of the volume of weathered material (regolith) that is generated with time. Hence, in our 0-dimensional model the volume of regolith exported from the orogen can be described as

$$E = \frac{CLRP}{dt} + \frac{W}{dt} - \frac{dR}{dt} \quad (3),$$

where $CLRP$ (*Coseismic Landslide Regolith Production*) is the average thickness (m) of weathered material generated by coseismic landslides, all of which is assumed to be transportable, W (m) is the thickness of rock weathering caused by all other mechanisms (simply the thickness of material removed from the bedrock when there is no regolith cover), and R is the thickness (m) of weathered material stored as mobile regolith. Combining the uplift and erosion equations allows us to track the change in two surfaces; the change in the topographic surface is

$$\frac{dS_T}{dt} = U_{co} + U_{as} - \frac{CLRP}{dt} - \frac{W}{dt} + \frac{dR}{dt} \quad (4);$$

The change in the surface that is composed of intact bedrock (S_B) can be described as

$$\frac{dS_B}{dt} = U_{co} + U_{as} - \frac{CLRP}{dt} - \frac{W}{dt} \quad (5);$$

And the change in regolith thickness is

$$\frac{dR}{dt} = \frac{CLRP}{dt} + \frac{W}{dt} - E \quad (6).$$

The model represents the average topographic surface uplift, regolith generation, and bedrock surface lowering for an area of that is set by the maximum area of displacement of the largest possible earthquake. As surface uplift rates for mountain ranges are hard to define (England and Molnar, 1990), we set the model to a flux steady state, where U is set to equal the long-term erosion rate (E). For each timestep in the model, an earthquake with $M_w > 5$ is randomly chosen from a power law distribution, and the coseismic uplift associated with this earthquake is calculated using an empirical scaling relationship (Li et al., 2014) between magnitude and uplift volume,

$$\log(V_u) = 1.06(\pm 0.22)M_w - 8.40(\pm 1.44) \quad (7),$$

where V_u is the volume of rock uplift generated by an earthquake of magnitude M_w and is scaled by α to calculate U_{co} . $M_w > 5$ earthquakes are the smallest that regularly produce coseismic landsliding and produce very little rock uplift (Marc et al., 2016b). We optimise the coseismic rock uplift within the setup of the model based on the relative importance of coseismic



145 and aseismic rock uplift (α) and to ensure flux steady state. The addition of different proportions of aseismic rock uplift has a material effect on the modelled topographic surface uplift by causing large earthquakes to lower the rock surface. The large earthquakes have their uplift reduced while the weathering they produce does not change, resulting in lowering.

Regolith is generated in the model based on calculations of bedrock lowering by CLRP and weathering by other mechanisms. Malamud's (Malamud et al., 2004) scaling of landslide volume (V_l) and earthquake magnitude (Figure 2A)

$$\log V_l = 1.42M_w - 11.26(\pm 0.52) \quad (8),$$

150 is converted to a depth of landsliding by dividing by the area of the model space (A). Alternative models of coseismic landslide volume as a function of seismic moment (Marc et al., 2016a; Robinson et al., 2016) cannot easily be scaled into a 0-dimensional model space due to their reliance upon earthquake source depth and landscape metrics. **These models describe the relationship between earthquake magnitude and total landslide volume as a curve around a hinge magnitude. This has the effect of reducing the importance of large earthquakes in the surface uplift balance.** All empirical models relating coseismic
155 landslide volume and earthquake magnitude have large uncertainties in them, we acknowledge these by applying a normal distribution of error using the uncertainty bounds on the landsliding volume produced by each earthquake (Figure 2A). The total new regolith generated by coseismic landslides is then calculated as the difference between the average depth of landsliding and the average thickness of the regolith. **Finally, all other weathering is calculated as the difference between the material removed from the mountain belt and CLRP.**

160 2.2 Model implementation: Longmen Shan

We test our model using the Longmen Shan due to the wealth of studies of the area both prior to and after the 2008 Wenchuan earthquake. These studies allow for the minimal parameters in our model to be well constrained. The Longmen Shan marks the eastern margin of the Tibetan plateau and the western edge of the Sichuan Basin (Li et al., 2017a). Hillslopes are at their threshold steepness with pervasive bedrock and limited channel storage, suggesting a **bedrock landscape** (Li et
165 al., 2014; Ouimet et al., 2009; Parker et al., 2011). The front of the range is dissected by three parallel dextral-thrust oblique-slip thrust faults, two of which, the Yingxiu-Beichuan and Pengguan faults, ruptured during the 2008 Wenchuan earthquake (Hubbard and Shaw, 2009; Li et al., 2016; Parker et al., 2011). Prior to this earthquake, geodetic measurements recorded limited shortening rates suggesting a role for lower crustal flow in driving surface uplift (Clark et al., 2005; Kirby et al., 2003; Royden et al., 1997; Wang et al., 2012). However, significant shortening associated with the Wenchuan earthquake
170 supports an important, possibly exclusively coseismic surface uplift element (Hubbard and Shaw, 2009).

To apply the model to the Longmen Shan we use a power law relationship derived from historical earthquake records: $\log_{10} N > M_w = 3.93 - 0.91M_w$ (Li et al., 2017b). As N_{\min} corresponds to $M_w=5$, we get a minimum return time of an earthquake of 5 years. This power law relationship is varied in some experiments to match the uncertainties in the return



175 time of Wenchuan sized earthquakes (Densmore et al., 2007; Li et al., 2014, 2017a). We use an apatite fission track-derived
exhumation rate of 0.62 (+0.14 -0.08) mm/yr (Li et al., 2017a) to represent the long-term erosion rate and sediment flux from
the orogen (E). We set the model domain length to equal the length of the fault and its width to the deformation caused by
the uplift of a M_w 8 earthquake (2600 km²), consistent with the historical record and the observation that the 2008 M_w 7.9
Wenchuan earthquake ruptured almost the entire length of the fault (Li et al., 2014, 2019). We ran the model for 25 Myr to
allow multiple analyses over various timescales, and varied α between 0 and 1.

180 2.3 Exhumation calculations within the model

We calculated exhumation for 2kyr intervals, which is the average time our model takes to exhume 1.2 m of rock through the
rock-regolith interface. This depth was chosen as broadly representing the recording timescale for cosmogenic radionuclides
(Gosse and Philips, 2001). Exhumation is calculated as the difference between rock uplift ($U_{co} + U_{as}$) and bedrock surface
uplift (S_B) over the recording time. We randomly chose 10,000 2kyr samples from our 25 Myr to produce a distribution of
185 exhumation rates. We performed two further numerical experiments: the first calculates exhumation rates for different
proportions of coseismic and aseismic rock uplift, while the second calculates denudation rates for decreasing maximum
earthquake magnitude.

2.4 Cosmogenic radionuclide calculations

We also calculate the cosmogenic ¹⁰Be flux out of the model through time. For each time step we add ¹⁰Be atoms to the
190 system using published production rates and attenuation lengths to simulate the depth profile of cosmogenic concentrations
(Balco et al., 2008; Braucher et al., 2011). After a **spin up** time of 10kyrs, the model tracks concentration of ¹⁰Be in the
sediment leaving the model. When an earthquake generates regolith the top part of the column is mixed, and the constant
erosional flux is applied to remove regolith from the surface. As erosion in the model is constant, and set to the long-term
exhumational flux, any change in concentration represents the effect of the stochastic exhumation of bedrock by EQTL.

195 3. Results and discussion

3.1 Coseismic landslide regolith production

Observations of the 2008 Wenchuan earthquake and its aftermath allow us to constrain export rate of landslide generated
regolith from mountain belts. Over 60,000 landslides were produced by the earthquake, a total volume of approximately 3
200 km³ (Li et al., 2014; Parker et al., 2011). Landslide deposits follow a power law magnitude frequency relationship where the
majority of landslides shorter than the hillslope length (Malamud et al., 2004; Marc et al., 2016a). The rate at which



landslide deposits can be evacuated from a catchment is typically related to the capacity of the fluvial system to transport the influx of sediment (Croissant et al., 2017; Yanites et al., 2010). However less than half of the total volume of the regolith produced by the Wenchuan earthquake is connected to the channel network immediately after the earthquake (Li et al., 2016). This lack of connectivity increases the residence time of regolith in the landscape due to the reliance on stochastic hillslope processes, such as debris flows for remobilisation into the channel (Croissant et al., 2019). The rapid stabilisation of the smallest landslides, many without being remobilised, indicates that a patchy regolith layer remains on the hillslope for much longer than a decade, likely centuries to millennia (Fan et al., 2018). Further extending the residence time of regolith within catchments is that many coseismic landslides occur within the upper parts of catchments where streams are small and have a low transport capacity, limiting their ability to transport the voluminous coarse landslide debris.

Within the model, regolith generated by the largest earthquakes can remain on hillslopes for ~1000 years (Figure 2A). The average thickness of new regolith that is produced in an earthquake (expressed as volume per area; i.e., a depth), is a strong function of both the pre-existing depth of regolith prior to new failures, the magnitude of the earthquake, and stochastic differences in the volume of landslides for a given earthquake magnitude (Figure 2B). The declining production rates with pre-existing regolith thickness result from the **armouring effect of the existing material**, which new landslides must cut down through before striking fresh rock. However, the distribution of earthquake frequencies exerts a stronger influence on total production through time, as more frequent small earthquakes can only ever weather small depths of regolith from the bedrock (Figure 2B). **The way coseismic landslide regolith production (CLRP) declines with existing regolith thickness is reminiscent of soil production functions described for environments without landsliding (Heimsath et al., 1997), and by analogy, we term the non-linear relationship between regolith production rate and the average depth of weathering by landslides seen here a coseismic landslide regolith production function (CLRPF). However, unlike a “traditional” soil production function, two elements of stochasticity are inherent to a CLRPF. One reflects the role of shielding of the bedrock surface (S_B) from lowering when the regolith layer is thicker than the average depth of the generated landslides (Larsen et al., 2010), and that thickness is dependent on the past history of landsliding in the model. The other reflects the inherent randomness in the size and distribution of the landslides that occur in response to an earthquake of a given magnitude, i.e., within equation (8).**

As expected, total seismic regolith production is dominated by the largest earthquakes which produce the largest mean landslide volumes (Malamud et al., 2004) (Figure 2B). Summing through time, earthquakes produce 42% of the total regolith generated by the model; $M_w > 7$ earthquakes account for ~65% of the total earthquake generated regolith and so 27% of the total regolith production. However, because smaller earthquakes occur much more often, **the average regolith layer is predominantly thin** – the modal thickness is only 0.02m, and the mean is 0.03m (Figure 2B inset). Thus, the model shows that although mountain belt regolith cover appears thin almost all the time, at times it can be thick enough to severely affect the short-term exhumation rates of the mountain range. **This result matches closely with observations of the Longmen Shan as a bedrock landscape with little storage** (Ouimet, 2010; Parker et al., 2011). Variability in the surface uplift through time (Figure 2C) is affected by the pre-earthquake regolith thickness and therefore the sequence of earthquakes which occur



before it. Where large earthquakes are closely spaced in time, **pre-existing regolith limits weathering of the bedrock surface**, encouraging uplift of the topographic surface. This interaction between surface uplift and regolith depth is controlled by: 1. the time between earthquakes; 2. the magnitude of the previous earthquake; and 3. the rate of regolith removal. If a **landscape has less frequent earthquakes, faster regolith removal and smaller earthquakes** a thin regolith layer is more likely (assuming that earthquakes are responsible for the majority of regolith generation) and the landscape will be less sensitive to the **CLRPF**.

3.2 Regolith generation by earthquakes and volume budgets

The contribution of earthquakes to the uplift and weathering budgets of mountains varies with earthquake magnitude, frequency, and the relative contribution of aseismic erosion, i.e., erosion not directly related to earthquakes such as **metrological triggered landsliding** and **oil production**. When coseismic rock uplift is the dominant uplift mechanism, we can classify **four distinct landscape response styles** at different earthquake magnitudes (Figure 3A). **On average, an earthquake of magnitude $M_w < 5.6$ lowers the topographic surface (S_T)**. Here, the **erosion flux out of the model** is greater than the rock uplift produced by the earthquakes (Figure 3A.1). For earthquakes with magnitudes $5.6 < M_w < 6.4$ the bedrock surface (S_B) rises because the rock uplift rate is greater than the typical regolith generation rate. The regolith thins because CLRPF is less than the erosional flux out of the model. (Figure 3A. (2)). CLRPF exceeds **erosional flux** in earthquakes with magnitudes $M_w > 6.4$. Earthquakes with $5.6 < M_w < 7.6$ (Figure 3A. (2-3)) cause net bedrock surface uplift. The largest earthquakes $> M_w > 7.6$ lower the bedrock surface due to the large volumes of regolith produced. However, much of the regolith is not removed before the next earthquake resulting in a **net topographic surface uplift**. For a purely aseismic uplift scenario, where earthquakes produce landslides but do not create rock uplift (Royden et al., 1997), earthquakes with $M_w > 6.5$ would cause bedrock surface lowering while smaller earthquakes would permit bedrock surface uplift due to low CLRPF. Earthquakes with $M_w > 6.5$ produce a thick layer of regolith which can persist until the next earthquake, limiting bedrock surface weathering and resulting in net uplift of the bedrock surface.

3.3 Earthquakes and exhumation

We explore how earthquakes affect the exhumation of mountain belts through direct calculation of exhumation of rock at the bedrock surface (S_B) relative to the topographic surface. First, to understand how stochastic earthquakes might affect exhumation rates, we measured the distribution of 10,000 randomly chosen exhumation rates averaged across 2kyrs years (the equivalent to the bedrock surface being lowered by ~1.2m). Large earthquakes create variability in exhumation rates. There is very little (~1%) variability in erosion rates in mountain ranges with earthquake magnitude $M_w < 5.0$. However, the introduction of stochastic weathering of many tens of cm of the bedrock surface by earthquakes with $M_w > 7$ introduces variability in exhumation. When large earthquakes are present, exhumation rates have a standard deviation of 0.055-0.081 mm/yr (9-14% of the long-term exhumation rate), and a range of 0.77-0.89 mm/yr, with the lower figures reflecting a greater



270 contribution of aseismic uplift (Figures 4A and 4B). Increasing the frequency of Wenchuan-like earthquakes from 4kyr to 500-year return produces more variable distributions of exhumation rates, with the standard deviation of exhumation rate increasing from 0.044 mm/yr (7% of long-term average) to 0.076 mm/yr (12% of the long-term average) (Figure 4C). Taken together, our model results suggest that up to 15% of the variability in a sample of exhumation rates from a single geographical region could be associated with the time since the last large ($M_w > 7.0$) earthquake. Pre-Wenchuan earthquake measurements of cosmogenically-derived erosion rates were between 40% and 60% lower than low-temperature thermochronometrically derived exhumation rates (Ouimet, 2010). Stochastic exhumation of low concentration bedrock by EQTL may explain some of that difference.

275 Cosmogenic radionuclides provide a record of potential earthquake-driven changes in exhumation because they have a relatively short averaging time that is close to the frequency of large earthquakes in many mountain belts. Our modelling results demonstrate the scale of stochastic variability in surface uplift and exhumation. We extended this analysis by simulating cosmogenic concentration in the model to estimate the potential impact of a large earthquake on both the cosmogenic concentration through time and the distribution of cosmogenic concentrations that are likely to be measured. We
280 **represent each earthquake as** thoroughly mixing the regolith down to its depth. The cosmogenic analysis (Figure 5B) shows that immediately after a large earthquake, mixing of low concentration bedrock material with higher concentration regolith lowers the concentration of radionuclides exiting the model. In the case of a representative magnitude M_w 8 earthquake, the concentration falls by around one third. However, the process of mixing also increases the concentration of nuclides close to the regolith-bedrock interface compared to the values before mixing, so that as the regolith is slowly eroded through time the
285 lower half releases concentrations *greater* than the long-term average. Therefore, in landscapes with frequent $M_w > 7$ earthquakes and regular long-term storage of regolith, **but with poor recording of major events**, it is possible to record more variable cosmogenic concentrations than might be expected, **including positive as well as negative excursions from the long-term mean.**

These modelling results provide testable predictions of the exhumation-related changes to cosmogenic concentration caused
290 by large earthquakes. Hence, we sought to examine whether the predicted variability might represent some of the variability associated with cosmogenic erosion rates in seismically active areas using global dataset compiled by Harel et al. (2016). Harel et al (2016) collated detrital cosmogenic ^{10}Be concentrations for 59 geographical areas, and recalculated the erosion rates using consistent production rate and shielding corrections. We compared the probability density distribution of erosion rates from within these geographic regions (limiting our samples to those with >18 measurements and basins larger than
295 10^5m^2 to limit sampling bias (Dingle et al., 2018; Niemi et al., 2005)) to seismicity, proxied using the 475 year return peak ground acceleration derived from a global seismic hazard map (Giardini et al., 1999; Harel et al., 2016) (Figure 6A). We then grouped these geographic regions into seismically active and inactive regions, noting the dominant sense of faulting, as this affects the distribution of coseismic landslides.

Seismically active landscapes had higher average cosmogenically-determined erosion rates with higher standard deviations
300 (Kruskal-Wallis H-test statistic=14.14, p-value=0.00017) (Figures 6A & 6B). The most seismically active mountain ranges



are also among the most varied in relief with some of the steepest catchments in the world. The variation of catchment steepness in a landscape correlates with denudation rates much more strongly than seismicity across the globe (Figure 6C). On average steeper basins in tectonically active landscapes could have higher landslide densities and larger volumes of coseismic generated regolith than shallower basins. This suggests that landscapes with more variation in basin form could enhance the temporal perturbations in denudation rates produced by earthquakes, but the contribution of tectonics to long term variation is difficult to isolate.

We further explored the role of averaging time by exploring how this may change with different contributions from seismic and aseismic uplift. After a large earthquake that produces tens of centimetres of instantaneous weathering of S_b , exhumation rates measured with different averaging times converge to the long-term mean rate within hundreds to thousands of years of a particular earthquake (Figure 5A). Bedrock surface exhumation rates are impacted by both surface uplift and lowering rates so as a result the time scale of the perturbation is impacted by the dominant form of uplift in the mountain range. As a result, the more dominant coseismic uplift is in a landscape, the longer the recording time needs to be before a reliable exhumation record can be made. Landscapes with more frequent earthquakes have more variable exhumation rates which require longer averaging times to achieve accurate measurements of the long-term average exhumation rate. Regardless of the frequency of earthquakes in a mountain range, the events of the greatest magnitude remain uncommon while being the dominant contributors to weathering. Hence the relationship between exhumation rate and averaging time is consistent with the Sadler effect that has been described for sedimentary systems (Schumer and Jerolmack, 2009). Unlike sedimentary systems, where it is possible to measure sedimentation rates from timescales of seconds to millions of years, there are few measures of exhumation that we can use and many of these have long averaging times. Thermochronometric methods average across timescales of 10^5 - 10^7 years, much longer than the averaging times of individual earthquakes. There is a possibility that cosmogenic radionuclide analysis may record individual earthquakes, where earthquake triggered landslides weather bedrock that has low cosmogenic concentration (Wang et al., 2017; West et al., 2014), although enhanced erosion during and immediately after an earthquake complicate the cosmogenic signal in practice.

Despite representing close to half of the weathering flux of mountain belts, stochastic earthquakes still remain missing substantively from our models of the development of mountains belts. The modelling here demonstrates that stochastic uplift and exhumation by large earthquakes is likely to be averaged across the timescale of most thermochronometers, with this temporal variability representing around 15% of the average exhumation rate. Even when a large earthquake occurs at the edge of a mountain belt, as has occurred in the Wenchuan region, the variable exhumation signal is further shredded by sediment transport by floods and debris flows, such that even sinks that are within 40 km of the epicentre show limited evidence for large earthquakes (Zhang et al., 2019). This suggests that the signal of a single earthquake could be discernible only within smaller basins immediately adjacent to the epicentre. Large basins (greater than $10,000\text{km}^2$) have been shown to be large enough to average out the perturbations caused by large landsliding events (Dingle et al., 2018; Marc et al., 2019). While these basins will offer reliable estimates of long-term erosion rates, the aim in this exercise is to identify variations from this, thus smaller basins could be suitable targets to recognise variations due to earthquakes. Our model suggests that



335 the impact of a large earthquake is not necessarily big enough to perturb the denudation rate of an orogen for the whole of a
cosmogenic nuclide recording time. The combination of averaging times, shredding, and the relative contributions of large
earthquakes to long term exhumation rates  help us to understand the lack of clear signatures for single earthquakes in
sedimentary or exhumation records.

4. Conclusions and implications

340 Our simulations show that the while the regolith generated by large earthquakes can reduce the rate of weathering and hence
exhumation, increasing uplift of the bedrock surface, the magnitude of this effect is small relative to the background rates of
rock uplift and the frequency distribution of earthquakes. These results demonstrate that background tectonic processes and
rates are the dominant control on the surface uplift, while the more important role for large earthquakes is their control on
weathering. Small earthquakes contribute very little to both uplift and weathering resulting in below average exhumation
345 being recorded when large earthquakes are unaccounted for. While large earthquakes do produce higher than average
exhumation rates, the slow and stochastic removal of regolith from the orogen reduces the magnitude and timescale of the
signal. The relatively long timescales of exhumation records prevent the recording of orogen scale variation due to a single
earthquake. A better understanding of the controls on bedrock weathering by earthquake triggered landslides is required to
identify signals of earthquakes in sedimentary records. Higher resolution exhumation records and the growing recognition of
350 the complex nature of sediment cascades will help to explore this problem.

Author Contributions

All authors contributed to the writing and ideas of the paper. XF, GS, OF designed the methodology for the collection and
analysis of the multitemporal landslide inventory; OF, DH, TCH, AH designed the model and experiment, which OF wrote;
TCH, XF, RH formulated the overall project aims.

355 Competing interests

The authors declare no competing financial interests.



Acknowledgements

The authors would like to thank Lanxin Dai, Qin Yang and others who contributed to the collection of the landslide inventory and acknowledge the funding of the Newton Fund, Natural Environmental Research Council, Economic and Social Research Council, and National Science Foundation for China grant, NE/N012240/.

References

- Avouac, J. P.: Dynamic Processes in Extensional and Compressional Settings – Mountain Building : From Earthquakes to Geological Deformation, *Treatise Geophys.*, 6, 377–439, 2007.
- Balco, G., Stone, J. O., Lifton, N. A. and Dunai, T. J.: A complete and easily accessible means of calculating surface exposure ages or erosion rates from ^{10}Be and ^{26}Al measurements, *Quat. Geochronol.*, 3(3), 174–195, doi:10.1016/j.quageo.2007.12.001, 2008.
- Bonilla, M. G., R.K., M. and Lienkaemper, J. J.: Statistical relations among earthquake magnitude, surface rupture length and surface fault displacement, *Bull. Seismol. Soc. Am.*, 74(6), 2379–2411, 1984.
- Braucher, R., Merchel, S., Borgomano, J. and Bourlès, D. L.: Production of cosmogenic radionuclides at great depth: A multi element approach, *Earth Planet. Sci. Lett.*, doi:10.1016/j.epsl.2011.06.036, 2011.
- Clark, M. K., Bush, J. W. M. and Royden, L. H.: Dynamic topography produced by lower crustal flow against rheological strength heterogeneities bordering the Tibetan Plateau, *Geophys. J. Int.*, 162(2), 575–590, doi:10.1111/j.1365-246X.2005.02580.x, 2005.
- Croissant, T., Lague, D., Steer, P. and Davy, P.: Rapid post-seismic landslide evacuation boosted by dynamic river width, *Nat. Geosci.*, 10(9), 680–684, doi:10.1038/ngeo3005, 2017.
- Croissant, T., Steer, P., Lague, D., Davy, P., Jeandet, L. and Hilton, R. G.: Seismic cycles, earthquakes, landslides and sediment fluxes: Linking tectonics to surface processes using a reduced-complexity model, *Geomorphology*, 339, 87–103, doi:10.1016/j.geomorph.2019.04.017, 2019.
- Densmore, A. L., Ellis, M. A., Li, Y., Zhou, R., Hancock, G. S. and Richardson, N.: Active tectonics of the Beichuan and Pengguan faults at the eastern margin of the Tibetan Plateau, *Tectonics*, 26(4), 1–17, doi:10.1029/2006TC001987, 2007.
- Densmore, A. L., Parker, R. N., Rosser, N. J., De Michele, M., Yong, L., Runqiu, H., Whadcoat, S. and Petley, D. N.: Reply to “Isostasy can’t be ignored,” *Nat. Geosci.*, 5(2), 83–84, doi:10.1038/ngeo1385, 2012.
- Dingle, E. H., Sinclair, H. D., Attal, M., Rodés, Á. and Singh, V.: Temporal variability in detrital ^{10}Be concentrations in a large Himalayan catchment, *Earth Surf. Dyn.*, 6(3), 611–635, doi:10.5194/esurf-6-611-2018, 2018.
- England, P. and Molnar, P.: Surface uplift, uplift of rocks, and exhumation of rocks, *Geology*, 18(12), 1173–1177, doi:10.1130/0091-7613(1990)018<1173:SUUORA>2.3.CO, 1990.
- Fan, X., Domènech, G., Scaringi, G., Huang, R., Xu, Q., Hales, T. C., Dai, L., Yang, Q. and Francis, O.: Spatio-temporal



- evolution of mass wasting after the 2008 Mw 7.9 Wenchuan Earthquake revealed by a detailed multi-temporal inventory, *Landslides*, (September), doi:10.1007/s10346-018-1054-5, 2018.
- 390 Giardini, D., Grunthal, G., Shedlock, K. M. and Peizhen, Z.: The GSHAP Global Seismic Hazard Map, *Ann. Di Geofis.*, 42(6), 1225–1230, 1999.
- Gosse, J. and Philips, F.: Terrestrial in situ cosmogenic nuclides: theory and application, *Quat. Sci. Rev.*, 20, 1475–1560, 2001.
- Hales, T. C., Abt, D. L., Humphreys, E. D. and Roering, J. J.: A lithospheric instability origin for Columbia River flood
395 basalts and Wallowa Mountains uplift in northeast Oregon, *Nature*, 438(7069), 842–845, doi:10.1038/nature04313, 2005.
- Harel, M., Mudd, S. M. and Attal, M.: Geomorphology Global analysis of the stream power law parameters based on worldwide Be denudation rates, *Geomorphology*, 268, 184–196, doi:10.1016/j.geomorph.2016.05.035, 2016.
- Heimsath, A. M., Dietrichs, W. E., Nishiizumi, K. and Finkel, R. C.: The soil production function and landscape equilibrium, *Nature*, 388(6640), 358–361, doi:10.1038/41056, 1997.
- 400 Hovius, N., Meunier, P., Lin, C. W., Chen, H., Chen, Y. G., Dadson, S., Horng, M. J. and Lines, M.: Prolonged seismically induced erosion and the mass balance of a large earthquake, *Earth Planet. Sci. Lett.*, 304(3–4), 347–355, doi:10.1016/j.epsl.2011.02.005, 2011.
- Howarth, J. D., Fitzsimons, S. J., Norris, R. J. and Jacobsen, G. E.: Lake sediments record cycles of sediment flux driven by large earthquakes on the Alpine fault, New Zealand, *Geology*, 40(12), 1091–1094, doi:10.1130/G33486.1, 2012.
- 405 Hubbard, J. and Shaw, J. H.: Uplift of the Longmen Shan and Tibetan plateau, and the 2008 Wenchuan ($M = 7.9$) earthquake, *Nature*, 458(7235), 194–197, doi:10.1038/nature07837, 2009.
- Jerolmack, D. J. and Paola, C.: Shredding of environmental signals by sediment transport, *Geophys. Res. Lett.*, 37(19), n/a–n/a, doi:10.1029/2010GL044638, 2010.
- Keefer, D. K.: The importance of earthquake-induced landslides to long-term slope erosion and slope-failure hazards in
410 seismically active regions, *Geomorphology*, 10(1–4), 265–284, doi:10.1016/0169-555X(94)90021-3, 1994.
- Kirby, E., Whipple, K. X., Tang, W. and Chen, Z.: Distribution of active rock uplift along the eastern margin of the Tibetan Plateau: Inferences from bedrock channel longitudinal profiles, *J. Geophys. Res. Solid Earth*, 108(B4), doi:10.1029/2001JB000861, 2003.
- Korup, O. and Clague, J. J.: Natural hazards, extreme events, and mountain topography, *Quat. Sci. Rev.*, 28(11–12), 977–
415 990, doi:10.1016/j.quascirev.2009.02.021, 2009.
- Larsen, I. J., Montgomery, D. R. and Korup, O.: Landslide erosion controlled by hillslope material, *Nat. Geosci.*, 3(4), 247–251, doi:10.1038/ngeo776, 2010.
- Li, G., West, A. J., Densmore, A. L., Jin, Z., Parker, R. N. and Hilton, R. G.: Seismic mountain building: Landslides associated with the 2008 Wenchuan earthquake in the context of a generalized model for earthquake volume balance,
420 *Geochemistry, Geophys. Geosystems*, 15(4), 833–844, doi:10.1002/2013GC005067, 2014.
- Li, G., West, A. J., Densmore, A. L., Hammond, D. E., Jin, Z., Zhang, F., Wang, J. and Hilton, R. G.: Connectivity of



- earthquake-triggered landslides with the fluvial network: Implications for landslide sediment transport after the 2008 Wenchuan earthquake, *J. Geophys. Res. Earth Surf.*, 121, 703–724, doi:10.1002/2015JF003718. Received, 2016.
- Li, G., West, A. J., Densmore, A. L., Jin, Z., Zhang, F., Wang, J., Clark, M. and Hilton, R. G.: Earthquakes drive focused denudation along a tectonically active mountain front, *Earth Planet. Sci. Lett.*, 472, 253–265, doi:10.1016/j.epsl.2017.04.040, 2017a.
- Li, G., West, A. J. and Qiu, H.: Competing effects of mountain uplift and landslide erosion over earthquake cycles, *J. Geophys. Res. Solid Earth*, 2018JB016986, doi:10.1029/2018JB016986, 2019.
- Li, Z., Liu-Zeng, J., Almeida, R., Hubbard, J., Sun, C. and Yi, G.: Re-evaluating seismic hazard along the southern Longmen Shan, China: Insights from the 1970 Dayi and 2013 Lushan earthquakes, *Tectonophysics*, 717(135), 519–530, doi:10.1016/j.tecto.2017.09.001, 2017b.
- Malamud, B. D., Turcotte, D. L., Guzzetti, F. and Reichenbach, P.: Landslides, earthquakes, and erosion, *Earth Planet. Sci. Lett.*, 229(1–2), 45–59, doi:10.1016/j.epsl.2004.10.018, 2004.
- Marc, O., Hovius, N., Meunier, P., Gorum, T. and Uchida, T.: A seismologically consistent expression for the total area and volume of earthquake-triggered landsliding, *J. Geophys. Res. Earth Surf.*, 121(4), 640–663, doi:10.1002/2015JF003732, 2016a.
- Marc, O., Hovius, N. and Meunier, P.: The mass balance of earthquakes and earthquake sequences, *Geophys. Res. Lett.*, 43(8), 3708–3716, doi:10.1002/2016GL068333, 2016b.
- Marc, O., Behling, R., Andermann, C., Turowski, J. M., Illien, L., Roessner, S. and Hovius, N.: Long-term erosion of the Nepal Himalayas by bedrock landsliding: the role of monsoons, earthquakes and giant landslides, *Earth Surf. Dyn.*, 7, 107–128, doi:10.5194/esurf-2018-69, 2019.
- Meade, B. J.: The signature of an unbalanced earthquake cycle in Himalayan topography?, *Geology*, 38(11), 987–990, doi:10.1130/G31439.1, 2010.
- Molnar, P.: Isostasy can't be ignored, *Nat. Geosci.*, 5(2), 83, doi:10.1038/ngeo1383, 2012.
- Molnar, P., England, P. and Martinod, J.: Mantle dynamics, uplift of the Tibetan plateau, and the Indian monsoon, *Rev. Geophys.*, 31(4), 357–396 [online] Available from: <http://www.agu.org/pubs/crossref/1993/93RG02030.shtml>, 1993.
- Molnar, P., England, P. C. and Jones, C. H.: Mantle dynamics, isostasy, and the support of high terrain, *J. Geophys. Res. Solid Earth Res.*, 120, 1932–1957, doi:10.1002/2014JB011724. Received, 2015.
- Niemi, N. A., Oskin, M., Burbank, D. W., Heimsath, A. M. and Gabet, E. J.: Effects of bedrock landslides on cosmogenically determined erosion rates, *Earth Planet. Sci. Lett.*, 237(3–4), 480–498, doi:10.1016/j.epsl.2005.07.009, 2005.
- Ouimet, W. B.: Landslides associated with the May 12, 2008 Wenchuan earthquake: Implications for the erosion and tectonic evolution of the Longmen Shan, *Tectonophysics*, 491(1–4), 244–252, doi:10.1016/j.tecto.2009.09.012, 2010.
- Ouimet, W. B., Whipple, K. X. and Granger, D. E.: Beyond threshold hillslopes: Channel adjustment to base-level fall in tectonically active mountain ranges, *Geology*, 37(7), 579–582, doi:10.1130/G30013A.1, 2009.
- Parker, R. N., Densmore, A. L., Rosser, N. J., De Michele, M., Li, Y., Huang, R., Whadcoat, S. and Petley, D. N.: Mass



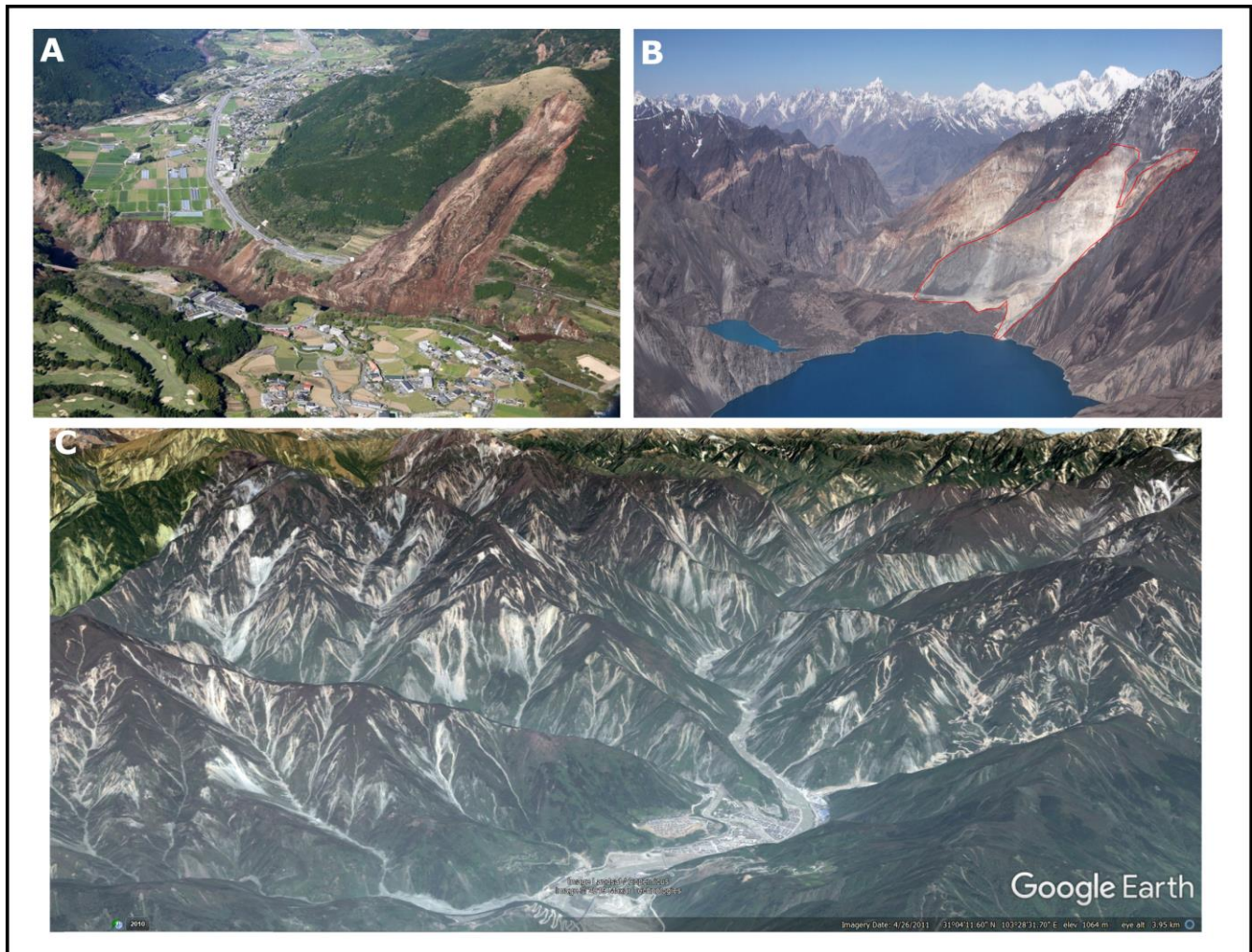
- wasting triggered by the 2008 Wenchuan earthquake is greater than orogenic growth, *Nat. Geosci.*, 4(7), 449–452, doi:10.1038/ngeo1154, 2011.
- Pearce, A. J., Watson, A. J. and Zealand, N.: Effects of earthquake-induced landslides on sediment budget and transport over a 50-yr period., *Geology*, 14, 52–55, 1986.
- 460 Roback, K., Clark, M. K., West, A. J., Zekkos, D., Li, G., Gallen, S. F., Chamlagain, D. and Godt, J. W.: The size, distribution, and mobility of landslides caused by the 2015 Mw7.8 Gorkha earthquake, Nepal, *Geomorphology*, 301, 121–138, doi:10.1016/j.geomorph.2017.01.030, 2018.
- Robinson, T. R., Davies, T. R. H., Wilson, T. M. and Orchiston, C.: Coseismic landsliding estimates for an Alpine Fault earthquake and the consequences for erosion of the Southern Alps, New Zealand, *Geomorphology*, 263, 71–86, doi:10.1016/j.geomorph.2016.03.033, 2016.
- 465 Royden, L. H., Burchfiel, B. C., King, R. W., Chen, Z., Shen, F. and Liu, Y.: Surface deformation and lower crust flow in eastern Tibet, *Science* (80-.), 276(788–790), 788–791, 1997.
- Schumer, R. and Jerolmack, D. J.: Real and apparent changes in sediment deposition rates through time, *J. Geophys. Res. Solid Earth*, 114(3), 1–12, doi:10.1029/2009JF001266, 2009.
- 470 Simpson, G.: Accumulation of permanent deformation during earthquake cycles on reverse faults, *J. Geophys. Res. Solid Earth*, 120(3), 1958–1974, doi:10.1002/2014JB011442, 2015.
- Stolle, A., Bernhardt, A., Schwanghart, W., Hoelzmann, P., Adhikari, B. R., Fort, M. and Korup, O.: Catastrophic valley fills record large Himalayan earthquakes, Pokhara, Nepal, *Quat. Sci. Rev.*, 177, 88–103, doi:10.1016/j.quascirev.2017.10.015, 2017.
- 475 Turcotte, D. L. and Schubert, G.: *Geodynamics*, Second edi., Cambridge University Press., 2002.
- Wang, E., Kirby, E., Furlong, K. P., Van Soest, M., Xu, G., Shi, X., Kamp, P. J. J. and Hodges, K. V.: Two-phase growth of high topography in eastern Tibet during the Cenozoic, *Nat. Geosci.*, 5(9), 640–645, doi:10.1038/ngeo1538, 2012.
- Wang, W., Godard, V., Liu-Zeng, J., Scherler, D., Xu, C., Zhang, J., Xie, K., Bellier, O., Ansberque, C. and de Sigoyer, J.: Perturbation of fluvial sediment fluxes following the 2008 Wenchuan earthquake, *Earth Surf. Process. Landforms*, 42(15), 480 2611–2622, doi:10.1002/esp.4210, 2017.
- Wells, D. L. and Coppersmith, Kevin, J.: New empirical relationship between magnitude, rupture length, rupture width, rupture area, and surface displacement, *Bull. Seismol. Soc. Am.*, 84(4), 974–1002, 1994.
- West, A. J., Hetzel, R., Li, G., Jin, Z., Zhang, F., Hilton, R. G. and Densmore, A. L.: Dilution of ^{10}Be in detrital quartz by earthquake-induced landslides: Implications for determining denudation rates and potential to provide insights into landslide sediment dynamics, *Earth Planet. Sci. Lett.*, 396, 143–153, doi:10.1016/j.epsl.2014.03.058, 2014.
- 485 Yanites, B. J., Tucker, G. E., Mueller, K. J. and Chen, Y.-G.: How rivers react to large earthquakes: Evidence from central Taiwan, *Geology*, 38(7), 639–642, doi:10.1130/G30883.1, 2010.
- Zhang, F., Jin, Z., West, A. J., An, Z., Hilton, R. G., Wang, J., Li, G., Densmore, A. L., Yu, J., Qiang, X., Sun, Y., Li, L., Gou, L., Xu, Y., Xu, X., Liu, X., Pan, Y. and You, C.-F.: Monsoonal control on a delayed response of sedimentation to the



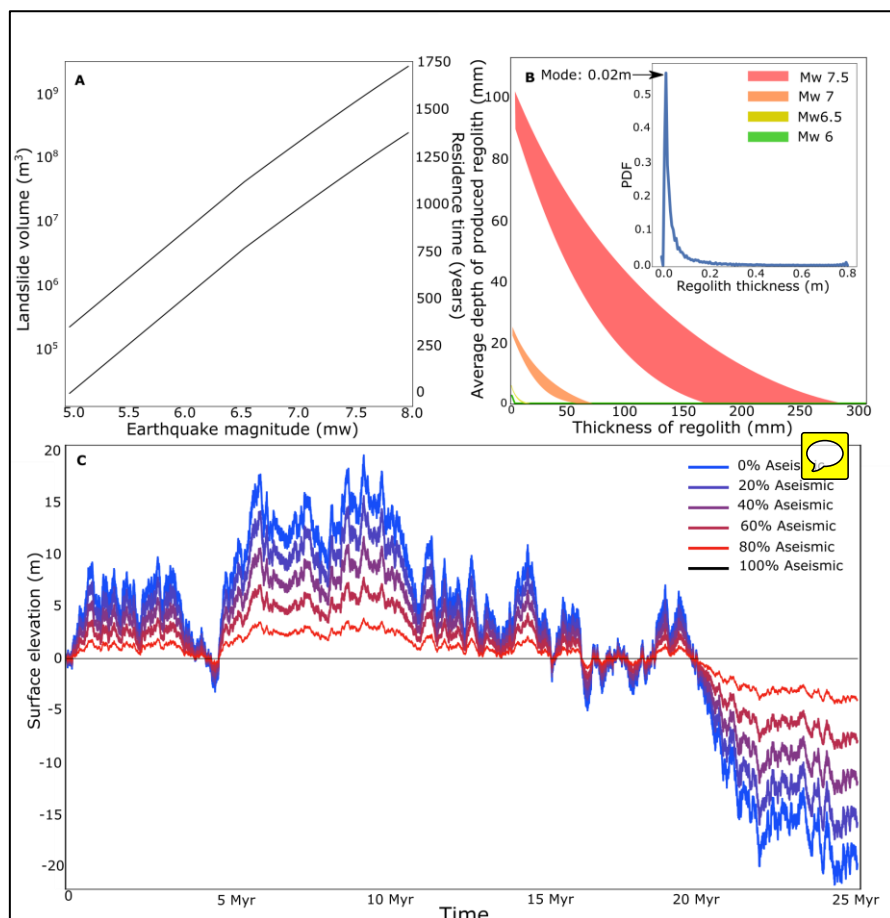
490 2008 Wenchuan earthquake, *Sci. Adv.*, 5(6), doi:10.1126/sciadv.aav7110, 2019.



Figures



495 Figure 1. Landslides in thick regolith can remobilise sediment while causing little erosion as seen in the 2016 Kumamoto
Earthquake (A). During earthquakes in landscapes with little pre-existing regolith, huge volumes of regolith can be generated
500 coseismically e.g., 1911 Usui Dam, Tajikistan, (Red line highlights the landslide scar) (B). The 2008 Wenchuan earthquake caused
more than 60,000 landslides (C), which have areas varying by many orders of magnitude. Some of the small landslides will
remobilise pre-existing regolith but the total volume of that remobilised regolith is unknown. Photo A sourced from
<https://blogs.agu.org/landslideblog>, Photo B from <https://www.mergili.at/worldimages/picture.php?/9330>, Photo C sourced from
Google Earth, using imagery provided by Landsat/Copernicus and Maxar Technologies, 2019 and draped over a digital terrain
model. © Google Earth



505

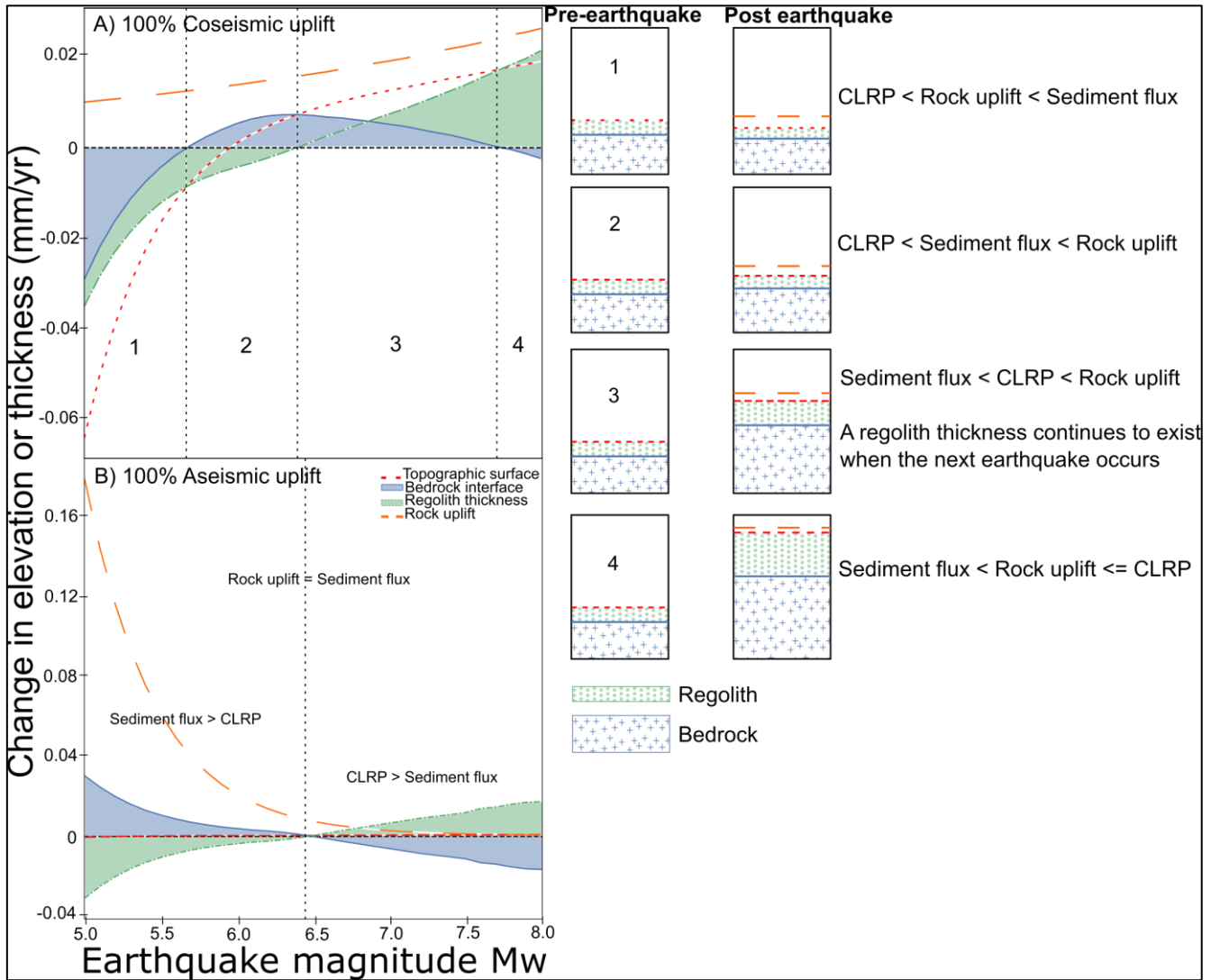
510

515

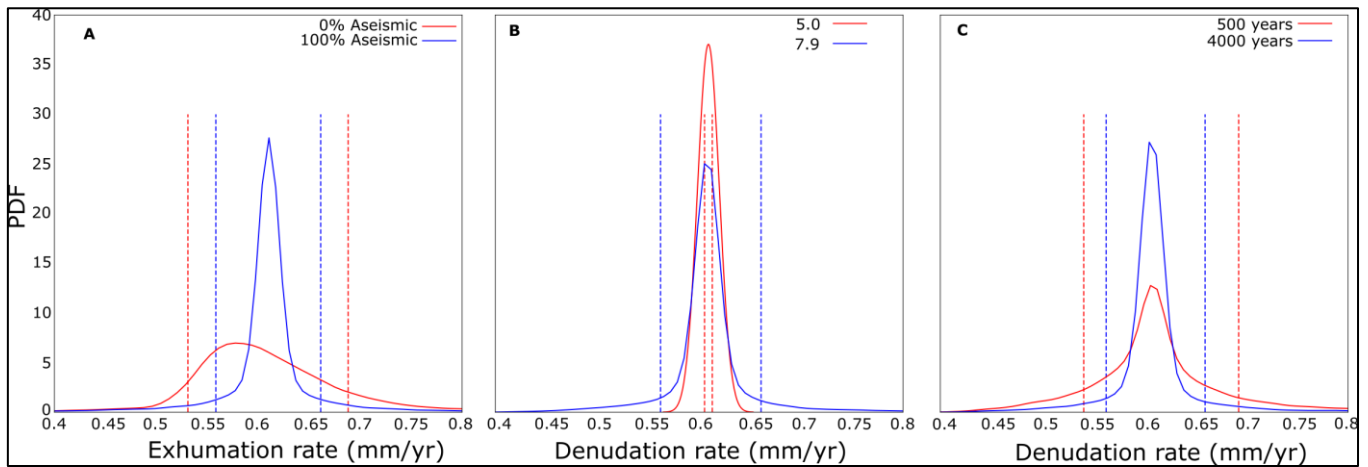
Figure 2. The average depth of regolith produced by an earthquake is impacted by its magnitude and the volume of regolith that is on the hillslope before the earthquake occurs. (A) Malamud (2004) scaling of landslide volume with magnitude and their average residence time in the Longmen Shan. The two lines represent the minimum and maximum volumes of landsliding generated, within the bounds on equation 8. (B) Variability of sediment production rates, expressed as volume per area, with existing depth of regolith on the hillslope, for four representative earthquake magnitudes. Coloured areas represent the variability of the landslide volume produced by an earthquake, randomly sampling from the bounds of equation 8. These Coseismic Landslide Regolith Production functions (CLRPF) emerge from the model rather than being set in advance, and the variability at each magnitude is driven by noise inherent in the relationship between magnitude and landslide size (equation 8). Inset shows the probability distribution function for regolith thickness across the whole model run, integrating the effects of the CLRPF through time. A small but nonzero spatially averaged modal regolith thickness persists, but significantly larger thicknesses regularly occur. (C) Variability of surface elevation through time for model runs with identical earthquake sequences, but with varying additional proportions of aseismic uplift. During times of thick regolith rapid surface uplift can occur despite the model being in a fixed flux steady state over longer timescales. Increasing the aseismic contribution to uplift reduces the uplift of large earthquakes, resulting in much less variable surface uplift and therefore exhumation.



520

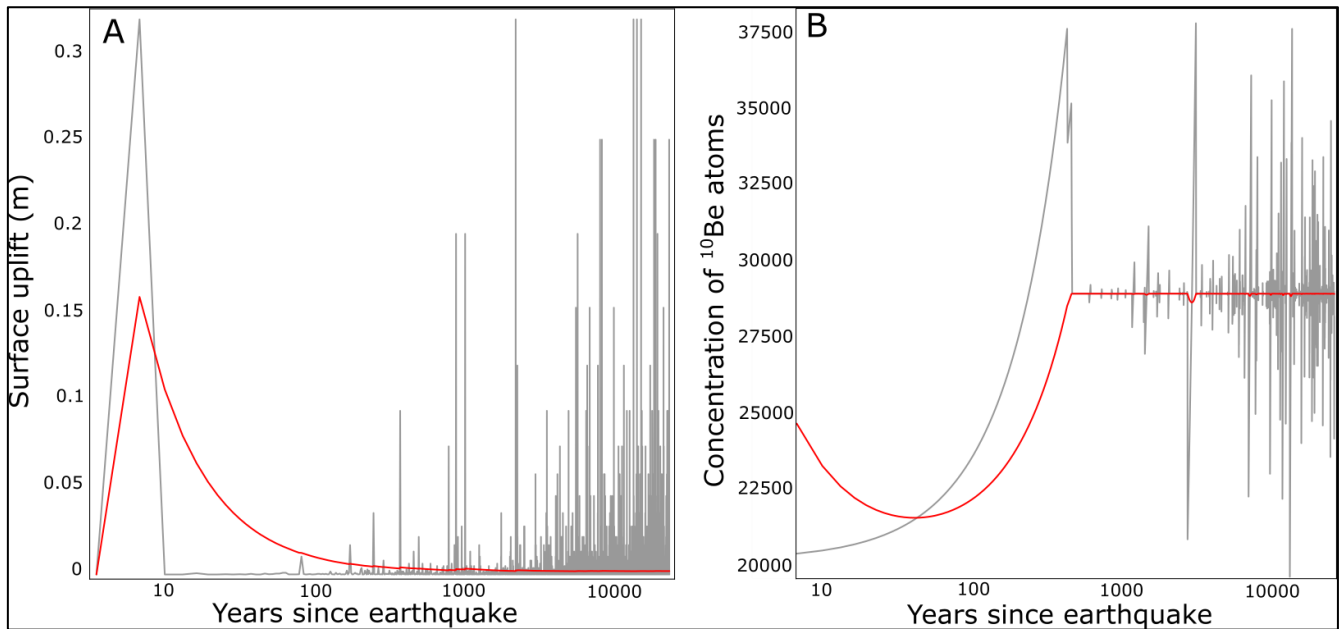


525 **Figure 3.** Interplay of changes to the modelled rock uplift rate, the topographic and bedrock surface uplifts, and the resulting regolith thickness through time, classified according to earthquake magnitude. The total bedrock and topographic uplift produced by each earthquake magnitude through the model run is summed up and divided by the run time to produce a rate. Each time a recorded surface intersects the horizontal axis we separate the chart into a zone which is further described in the text and cartoons. The top graph represents a run with 100% coseismic uplift while the bottom is purely aseismic.

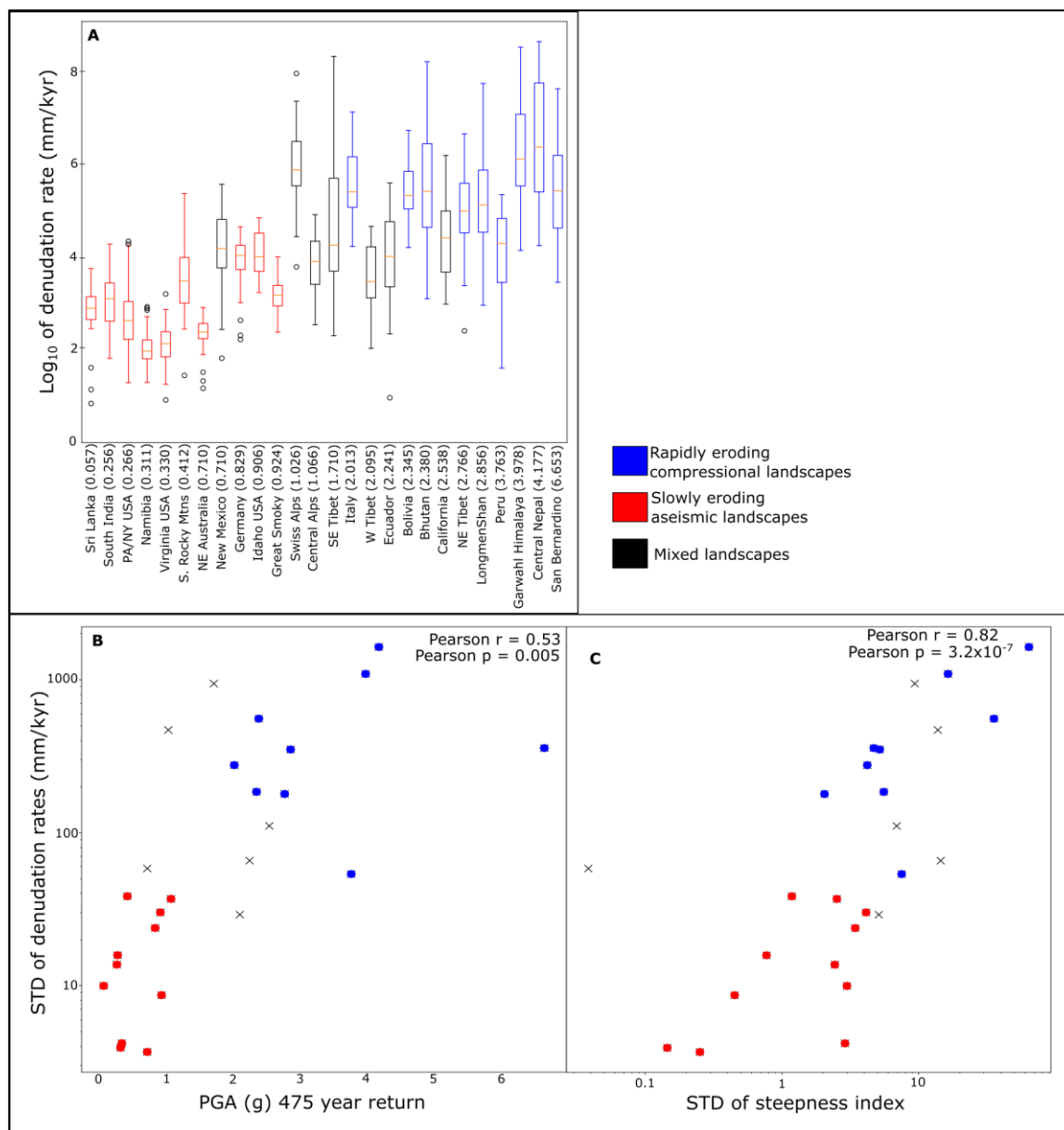


530 **Figure 4. Variation of exhumation and denudation rates in various scenarios. Dashed lines indicate the position of the mean +/- the**
standard deviation of the distribution. A) Exhumation rates in different uplift regimes. B) Denudation rates while varying the
maximum earthquake magnitude in a run. C) Denudation rates while varying the frequency of Wenchuan size earthquakes from
every 500 to every 4000 years.

535



540 **Figure 5. Variability of (A) Topographic surface uplift and (B) the recorded concentration of cosmogenic nuclides leaving the orogen after a representative magnitude 8 earthquake within the model run. Red lines are running means while the grey is the real time change caused by individual subsequent earthquakes.**



545 **Figure 6.** Reanalysis of detrital cosmogenic radionuclide derived denudation rates for mountain belts around the world compiled
 by Harel et al (2016), in the context of peak ground acceleration and tectonic environment. (A) A box plot indicating the median
 (central orange line), quartiles (end of box) and the range (“the whiskers”) of denudation rates in the analysed localities ordered by
 their average seismicity (in brackets), defined as the maximum Peak Ground Acceleration of a 475-year return period (PGA).
 Points indicate values outside the range, Median $\pm 1.5IQR$. (B) Standard deviation (STD) of denudation rates for each mountain
 550 belt against seismicity. (C) Standard deviation of denudation rates for each mountain belt compared to the standard deviation of
 steepness indexes. Steepness index is the relationship between slope and drainage area (k) which is normalised by a reference
 concavity to allow global comparison. The areas of highest variability are found in steep, tectonically active mountain ranges.